5406 *Chem. Mater.* **2009,** *21,* 5406–5412
DOI:10.1021/cm9014749

CHEMISTRY OF MATERIALS
Article

Immobilization of Alkali Metal Ions in a 3D Lanthanide-Organic Framework: Selective Sorption and H_2 Storage Characteristics

Sudip Mohapatra,[†] K. P. S. S. Hembram,[‡] Umesh Waghmare,[‡] and Tapas Kumar Maji*[,†]

[†]*Molecular Materials Laboratory, Chemistry and Physics of Materials Unit and* [‡]*Theoretical Sciences Unit, Jawaharlal Nehru Centre for Advanced Scientific Research, Jakkur, Bangalore 560064, India*

Received May 29, 2009. Revised Manuscript Received September 10, 2009

A lanthanide-alkali ($Ho^{III}-K^{I}$) bimetallic α-Po type 3D framework $\{KHo(C_2O_4)_2(H_2O)_4\}_n$ (**1**) ($C_2O_4^{2-}$ = oxalate dianion) has been synthesized and structurally characterized. Its dehydrated framework **1′**, after removal of the K-bound water molecules, is found to exhibit permanent porosity with a clear size selective vapor sorption properties and H_2 storage capability. High heat of H_2 sorption (approximately −10 kJ/mol) observed in experiment is shown to arise from the preferential interaction of H_2 with unsaturated K^{I} sites decorated on the pore surfaces, using first-principles density functional theory-based calculations of energetics as well as the detailed structure. Our work shows that a material with better hydrogen storage and release properties can be developed through immobilization of unsaturated reactive alkali metal ions at the pore surfaces in a metal-organic framework.

Introduction

Recent years, the synthesis and characterization of porous coordination polymers (PCPs) or metal-organic frameworks (MOFs) based on *d*-block metal ions and versatile organic linkers attracted considerable interest due to its applications in gas storage,[1] selective separation,[2] ion exchange,[3] catalysis,[4] and in molecular recognition properties.[5] In this context, analogous chemistry of MOFs with lanthanide (Ln) ions are attractive because of their versatile coordination geometry,[6] unique luminescent[7] and magnetic properties,[8] and possible high framework stability.[9] Ln-based MOFs typically contain solvent molecules for the gratification of higher coordination number of Ln and removal of these ancillary solvent molecules from the coordination sphere often results collapse of the framework. Therefore, Ln-frameworks without coordinated solvent molecules may exhibit high thermal stability and framework rigidity, which are essential for porous functionality. To date, only a handful of examples of Ln-organic frameworks with porous functionality have been reported.[10]

*Corresponding author. E-mail: tmaji@jncasr.ac.in. Phone: (+91) 80 2208 2826. Fax: (+91) 80 2208 2766.

(1) (a) Rowsell, J. L. C.; Yaghi, O. M. *Angew. Chem., Int. Ed.* **2005**, *44*, 4670. (b) Sun, S. D.; Simmons, J. M.; Collier, C. D.; Yuan, D.; Zhou, H. −C. *J. Am. Chem. Soc.* **2007**, *130*, 1012. (c) Férey, G. *Chem. Soc. Rev.* **2008**, *37*, 191. (d) Millward, A. R.; Yaghi, O. M. *J. Am. Chem. Soc.* **2005**, *127*, 17998.

(2) (a) Seo, J. S.; Whang, D.; Lee, H.; Jun, S. I.; Oh, J.; Jeon, Y. J.; Kim, K. *Nature* **2000**, *404*, 982. (b) Evans, O. R.; Ngo, H. L.; Lin, W. *J. Am. Chem. Soc.* **2001**, *123*, 10395. (c) Lee, J. Y.; Olson, D. H.; Pan, L.; Emge, T. J.; Li, J. *Adv. Funct. Mater.* **2007**, *17*, 1255. (d) Ngo, H. L.; Lin, W. *J. Am. Chem. Soc.* **2002**, *124*, 14298.

(3) (a) Maji, T. K.; Matsuda, R.; Kitagawa, S. *Nat. Mater.* **2007**, *6*, 142. (b) Min, K. S.; Suh, M. P. *J. Am. Chem. Soc.* **2000**, *122*, 6834. (c) Yaghi, O. M.; Li, H. *J. Am. Chem. Soc.* **1996**, *118*, 295.

(4) (a) Wu, C. D.; Hu, A.; Zhang, L.; Lin, W. *J. Am. Chem. Soc.* **2005**, *127*, 8940. (b) Ohmori, O.; Fujita, M. *Chem. Commun.* **2004**, *10*, 1586. (c) Dewa, T.; Siki, T.; Aoyama, Y. *J. Am. Chem. Soc.* **2001**, *123*, 502.

(5) Kido, J.; Okamoto, Y. *Chem. Rev.* **2002**, *102*, 2357.

(6) (a) Guillou, O.; Daiguebonne, C. *Handbook on the Physics and Chemistry of Rare Earths*; Gschneidner, K. A., Bünzli, J.-C. G., Pecharsky, V. K., Eds.; Elsevier: New York, 2005; Vol. *34*. (b) Cahill, C. L.; de Lill, D. T.; Frisch, M. *CrystEngComm.* **2007**, *9*, 15.

(7) (a) Guo, X.; Zhu, G.; Fang, Q.; Xue, M.; Tian, G.; Sun, J.; Li, X.; Qiu, S. *Inorg. Chem.* **2005**, *44*, 3850. (b) Moore, E. G.; Xu, J.; Jocher, C. J.; Castro-Rodriguez, I.; Raymond, K. N. *Inorg. Chem.* **2008**, *47*, 3105. (c) Wu, J. Y.; Yeh, T. T.; Wen, Y. S.; Twu, J.; Lu, K. L. *Cryst. Growth Des.* **2006**, *6*, 467. (d) Fratini, A.; Richards, G.; Larder, E.; Swavey, S. *Inorg. Chem.* **2008**, *47*, 1030. (e) Zhu, W. H.; Wang, Z. M.; Gao, S. *Inorg. Chem.* **2007**, *46*, 1337. (f) Thirumurugan, A.; Natarajan, S. *J. Mater. Chem.* **2005**, *15*, 4588.

(8) (a) Benelli, C.; Gatteschi, D. *Chem. Rev.* **2002**, *102*, 2369. (b) Bao-Qing, M.; Gao, S.; Su, G.; Xu, G. X. *Angew. Chem., Int. Ed.* **2001**, *40*, 434. (c) Costes, J. P.; Clemente-Juan, J. M.; Dahan, F.; Nicodeme, F.; Verelst, M. *Angew. Chem., Int. Ed.* **2002**, *41*, 323. (d) Hsu, C. F.; Lin, S. H.; Wei, H. H. *Inorg. Chem. Commun.* **2005**, *8*, 1128. (e) Costes, J. P.; Juan, J. M. C.; Dahan, F.; Nicodeme, F. *Dalton Trans.* **2003**, 1272. (f) Manna, S. C.; Zangrando, E.; Bencini, A.; Benelli, C.; Ray Chaudhuri, N. *Inorg. Chem.* **2006**, *45*, 9114.

(9) (a) Paz, F. A. A.; Klinowski, J. *Chem. Commun.* **2003**, *9*, 1484. (b) He, Z.; Gao, E. Q.; Wang, Z. M.; Yan, C. H.; Kurmoo, M. *Inorg. Chem.* **2005**, *44*, 862. (c) Zheng, X.; Sun, C.; Lu, S.; Liao, F.; Gao, S.; Jin, L. *Eur. J. Inorg. Chem.* **2004**, 3262.

(10) (a) Maji, T. K.; Mostafa, G.; Chang, H. −C.; Kitagawa, S. *Chem. Commun.* **2005**, 2436. (b) Pan, L.; Adams, K. M.; Hernandez, H. E.; Wang, X.; Zheng, C.; Hattori, Y.; Kaneko, K. *J. Am. Chem. Soc.* **2003**, *125*, 3062. (c) Zhao, J.; Long, L. S.; Huang, R. B.; Zheng, L. S. *Dalton Trans.* **2008**, 4714. (d) Dimos, A.; Tsaousis, D.; Michaelides, A.; Skoulika, S.; Golhen, S.; Ouahab, L.; Didierjean, C.; Aubry, A. *Chem. Mater.* **2002**, *14*, 2616. (e) Serre, C.; Ferey, G. *J. Mater. Chem.* **2002**, *12*, 3053. (f) Reineke, T. M.; Eddaoudi, M.; O'Keeffe, M.; Yaghi, O. M. *Angew. Chem., Int. Ed.* **1999**, *38*, 2590. (g) Rosi, N. L.; Kim, J.; Eddaoudi, M.; Chen, B.; O'Keeffe, M.; Yaghi, O. M. *J. Am. Chem. Soc.* **2005**, *127*, 1504. (h) Devic, T.; Serre, C.; Auderbrand, N.; Marrot, J.; Férey, G. *J. Am. Chem. Soc.* **2005**, *127*, 12788. (i) Luo, J.; Xu, H.; Liu, Y.; Zhao, Y.; Daemen, L.; Brown, C.; Timofeeva, T. V.; Ma, S.; Zhou, H. −C. *J. Am. Chem. Soc.* **2008**, *130*, 9626. (j) Millange, F.; Serre, C.; Marrot, J.; Gardant, N.; Pellé, F.; Férey, G. *J. Mater. Chem.* **2004**, *14*, 642. (k) Yue, Q.; Yang, J.; Li, G. −H.; Li, G. −D.; Chen, J. −S. *Inorg. Chem.* **2006**, *45*, 4431. (l) Guo, X.; Zhu, G.; Li, Z.; Sun, F.; Yang, Z.; Qiu, S. *Chem. Commun.* **2006**, 3172.

 Published on Web 10/28/2009

Storage of H_2 in a safe, compact, and convenient way represents an important current challenge for its use as an alternative fuel.[11] Nanostructured carbon materials and metal hydrides were extensively studied as potential adsorbents for H_2 storage.[12] Recently, MOFs with tunable pore sizes and chemical environment, have been found to exhibit promising H_2-storage materials.[13] Ideally, for practical use, the materials should exhibit quick uptake and release of the H_2 at ambient condition. High H_2-storage capacity (7.5 wt %) in MOF at 77 K was recently reported,[13c] but to extend the performance to ambient temperature, substantial improvement will be required in the heat of adsorption value. One of the strategies is to embed coordinatively unsaturated metal sites on the pore surfaces, which can interact more strongly than that the weak dispersion forces or H-bonding interactions. Evidence of stronger binding of H_2 to the $Cu^{2+}/Ni^{2+}/Mn^{2+}$ open metal sites have been reported[14a−f] and theoretical calculations also suggest higher interaction energy of H_2 with the unsaturated sites.[14g−j] Moreover, immobilization of the unsaturated alkali metal cations in the porous framework will exhibit interesting functionality based on strong charge-quadrupole interactions.[14i]

Recently, Shimizu et al. reported porous luminescent bimetallic (Ln-alkali)-organic frameworks synthesized in a stepwise manner using the lanthanide-organic metalloligand, which is finally attached to the alkali metal centers.[15] However, bimetallic coordination framework using Ln and alkali metal ions are very few and their porous functionalities are rarely observed.[16] Moreover, framework decorated with unsaturated alkali metal ions will provide ideal scaffold for more specific and strong binding sites for adsorbates, particularly for H_2.[14i] Hupp et al. recently demonstrated significant high uptake of H_2 by doping alkali metal cations in a redox active porous framework.[17] They observed H_2 uptake increases with dopant cation size, and remarkable 65% increase over uptake in K^I-doped sample compare to the assynthesized framework. In this article, we report synthesis and structural characterization and porous functionalities of a 3D bimetallic ($Ho^{III}-K^I$) framework, $\{KHo(C_2O_4)_2(H_2O)_4\}_n$ (**1**). The dehydrated solid of **1** (**1′**) shows permanent porosity as well as size-selective vapor (H_2O, MeOH, CH_3CN, and EtOH) sorption properties and interesting H_2 storage characteristics with high heat of adsorption value (−9.21 kJ/mol). Using first-principles calculations, we confirm this energy quantitatively, and uncover the nature of H_2-lattice interaction from the detailed structures determined for various sites of interaction. We show that K^I is the favorable site for H_2 adsorption.

Experimental Section

Materials. All the reagents were commercially available and used as supplied without further purification. $Ho(NO_3)_3\cdot 5H_2O$ and oxalic acid dihydrate ($H_2C_2O_4\cdot 2H_2O$) were obtained from Aldrich Chemical Co.

Synthesis of $\{KHo(C_2O_4)_2(H_2O)_4\}_n$ (1). A mixture of $Ho(NO_3)_3\cdot 5H_2O$ (0.220 g, 0.5 mmol), $H_2C_2O_4\cdot 2H_2O$ (0.111 g, 0.75 mmol), KOH (0.084 g, 1.5 mmol), and 10 mL of distilled water was placed in a 25 mL beaker, and the whole reaction solution was stirred for 1 h. The reaction mixture was then transferred into a 23 mL Teflon-lined stainless steel autoclave and heated at 150 °C for 120 h. The mixture was allowed to cool to room temperature. Colorless block-shaped single crystals suitable for X-ray study were separated manually from the white powder. (Yield 25%). IR (KBr cm^{-1}); 3526 br (OH); 1621 br s (COO); 1326 s(COO). Anal. Calcd. for $C_4H_8HoKO_{12}$: C, 10.61; H, 1.76. Found: C, 10.69; H, 1.54%. Single phase white crystalline powder of $\{KHo(C_2O_4)_2(H_2O)_4\}$ (**1**) were isolated in hydrothermal reaction by heating a mixture of $Ho(NO_3)_3\cdot 5H_2O$ (1 mmol, 0.441 g), $K_2C_2O_4\cdot H_2O$ (0.368 g, 2 mmol) at 180 °C for 200 h in a 23 mL Teflon-lined stainless steel autoclave. (Yield 85%). The phase purity was confirmed by the elemental analysis and PXRD measurements.

Physical Measurements. The elemental analysis was carried out on a Perkin-Elmer 1800 instrument. IR spectra were recorded on a Bruker IFS 66v/S spectrophotometer with samples prepared in KBr pellets in the region 4000−400 cm^{-1}. X-ray powder diffraction (PXRD) pattern were recorded on a Bruker D8 Discover instrument using Mo Kα radiation.

Adsorption Measurements. N_2 (77 K), CO_2 (195 and 298 K), and H_2 (77 K) adsorption study of the dehydrated samples prepared at 423 K under high vacuum, were carried out using QUANTACHROME AUTOSORB-1C analyzer. The adsorption isotherm of different solvents (like H_2O, CH_3CN, EtOH at

(11) (a) Schlapbach, L.; Züttel, A. *Nature* **2001**, *414*, 353. (b) Schlapbach, L. *MRS Bull*. **2002**, 675.
(12) (a) Liu, C.; Fan, Y. Y.; Liu, M.; Cong, H. T. *Science* **1999**, *286*, 1127.(b) Dillon, A. C.; Jones, K. M.; Bekkedahl, T. A.; Kiang, C. H.; Bethune, D. S.; Heben, M. J. **1997**, *386*, 377; (c) Grochala, W.; Edwards, P. P. *Chem. Rev*. **2004**, *104*, 1283. (d) Gundiah, G.; Govindraj, A.; Rajalakshmi, N.; Dhathathreyan, K. S.; Rao, C. N. R. *J. Mater. Chem*. **2003**, *13*, 209.
(13) (a) Park, H. J.; Suh, M. P. *Chem.—Eur. J*. **2008**, *14*, 8812. (b) Lin, X.; Jia, J.; Zhao, X.; Thomas, K. M.; Blake, A. J.; Walker, G. S.; Champness, N. R.; Hubberstey, P.; Schröder, M. *Angew. Chem., Int. Ed*. **2006**, *45*, 7358. (c) Wong Foy, A. G.; Matzger, A. J.; Yaghi, O. M. *J. Am. Chem. Soc*. **2006**, *128*, 3494. (d) Rowsell, J. L. C.; Millward, A. R.; Park, K. S.; Yaghi, O. M. *J. Am. Chem. Soc*. **2004**, *126*, 5666. (e) Latroche, M.; Surblé, S.; Serre, C.; Mellot-Draznieks, C.; Llewellyn, P. L.; Lee, J. −H.; Chang, J. S.; Jhung, S. H.; Férey, G. *Angew. Chem., Int. Ed*. **2006**, *45*, 8227. (f) Dailly, A.; Vajo, J. J.; Ahn, C. C. *J. Phys. Chem. B* **2006**, *110*, 1099. (g) Pan, L.; Sander, M. B.; Huang, X.; Li, J.; Smith, M.; Bittner, E.; Bockrath, B.; Johnson, J. K. *J. Am. Chem. Soc*. **2004**, *126*, 1308. (h) Chun, H.; Dybtsev, D. N.; Kim, H.; Kim, K. *Chem.—Eur. J*. **2005**, *11*, 3521. (i) Yang, W.; Lin, X.; Junhua, J.; Blake, A. J.; Wilson, C.; Hubberstey, P.; Champness, N. R.; Schroder, M. *Chem. Commun*. **2008**, 359. (k) Steven, K. S.; Long, J. R. *J. Am. Chem. Soc*. **2005**, *127*, 6507. (l) Uemura, K.; Maeda, A.; Maji, T. K.; Kanoo, P.; Kita, H. *Eur. J. Inorg. Chem*. **2009**, 2329.
(14) (a) Chen, B.; Ockwig, N. W.; Milward, A. R.; Contreras, D. S.; Yaghi, O. M. *Angew. Chem., Int. Ed*. **2005**, *44*, 4745. (b) Forster, P. M.; Eckert, J.; Chang, J. S.; Park, S. E.; Férey, G.; Cheetham, A. K. *J. Am. Chem. Soc*. **2003**, *125*, 1309. (c) Dinca, M.; Dailly, A.; Liu, Y.; Brown, C. M.; Neumann, D. A.; Long, J. R. *J. Am. Chem. Soc*. **2006**, *128*, 16876. (d) Liu, Y.; Kabbour, H.; Brown, C. M.; Neumann, D. A.; Ahn, C. C. *Langmuir* **2008**, *24*, 4772. (e) Panella, B.; Hirscher, M.; Pütter, H.; Müller, U. *Adv. Funct. Mater*. **2006**, *16*, 520. (f) Yang, Q.; Zhong, C. *J. Phys. Chem. B*. **2006**, *110*, 655. (g) Zhou, W.; Wu, H.; Yildirim, T. *J. Am. Chem. Soc*. **2008**, *130*, 15268. (h) Jonathan, L. B.; Abraham, C. S.; Eddaoudi, M.; Brian, S. *J. Am. Chem. Soc*. **2007**, *129*, 15202. (i) Han, S. S.; Goddard, W. A.III. *J. Am. Chem. Soc*. **2007**, *129*, 8422. (j) Zhou, W.; Yildirim, T. *J. Phys. Chem. C*. **2008**, *112*, 8132.
(15) (a) Chandler, D.; Yu, J. O.; Cramb, D. T.; Shimizu, G. K. H. *Chem. Mater*. **2007**, *19*, 4467. (b) Chandler, D.; Cramb, D. T.; Shimizu, G. K. H. *J. Am. Chem. Soc*. **2006**, *128*, 10403.
(16) (a) Zhang, X.; Xing, Y.; Wang, C.; Han, J.; Li, J.; Ge, M.; Zeng, X.; Niu, S. *Inorg. Chim. Acta* **2009**, *362*, 1058. (b) Bataille, T.; Auffrdic, J. −P.; Lour, D. *Chem. Mater*. **1999**, *11*, 1559.
(17) (a) Mulfort, K. L.; Farha, O. K.; Stern, C. L.; Sarjeant, A. A.; Hupp, J. T. *J. Am. Chem. Soc*. **2009**, *131*, 3866. (b) Mulfort, K. L.; Hupp, J. T. *Inorg. Chem*. **2008**, *47*, 7936.

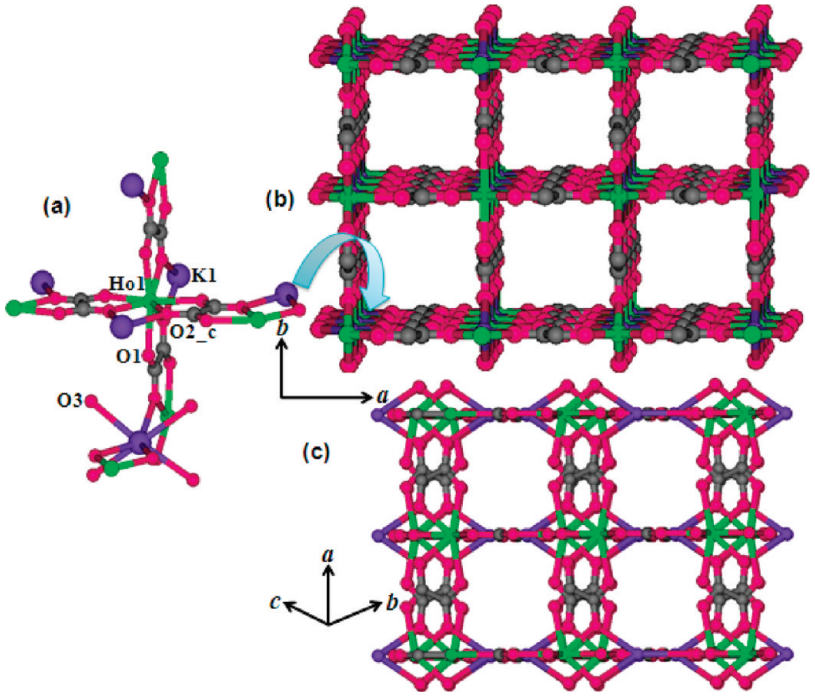

Figure 1. (a) View of the coordination environment of Ho^{III} and K^{I} in $\{KHo(C_2O_4)_2(H_2O)_4\}_n$ (**1**); (b) view of the 3D framework of **1** showing square shaped channel along the crystallographic *c*-axis; (c) view of the 3D framework along parallel to *a*-axis showing small channels. K-bound water molecules were removed.

298 K, and MeOH at 293 K) were measured in the vapor state by using BELSORP-aqua volumetric adsorption instrument from BEL, Japan. In the sample chamber (~12 mL) maintained at $T \pm 0.03$ K was placed the adsorbent sample (100−150 mg), which had been prepared at 493 K at 1×10^{-1} Pa for 18 h prior to measurement of the isotherms. The adsorbate was charged into the sample tube, and then the change of the pressure was monitored and the degree of adsorption was determined by the decrease of the pressure at the equilibrium state. All operations were computer-controlled and automatic. High-pressure hydrogen sorption isotherm measurements at 77 and 195 K and CO_2 sorption isotherm measurement at 298 K were carried out on a fully computer controlled volumetric BELSORP-HP, BEL JAPAN high-pressure instrument. The hydrogen and CO_2 used for the high pressure measurements is scientific/research grade with 99.999% purity. For the measurements, approximately 1.00 g sample was taken in a stainless-steel sample holder and degassed at 423 K for a period of 18 h under a 0.1 Pa vacuum. Dead volume of the sample cell was measured with helium gas of 99.999% purity. Nonideal correction for hydrogen and carbon dioxide gas were made by applying virial coefficients at the respective measurement temperature.

X-ray Crystallography. A suitable single crystal of compound **1** was mounted on a thin glass fiber with commercially available super glue. X-ray single crystal structural data were collected on a Bruker Smart−CCD diffractometer equipped with a normal focus, 2.4 kW sealed tube X-ray source with graphite monochromated Mo-*K*α radiation (λ = 0.71073 Å) operating at 50 kV and 30 mA, with ω scan mode. The program SAINT was used for integration of diffraction profiles and absorption correction were made with SADABS program. All the structures were solved by direct methods using SIR-92 and followed by successive Fourier and difference Fourier Syntheses. All the non-hydrogen atoms were refined anisotropically. All calculations were carried out using SHELXL 97,[18] SHELXS 97,[19] PLATON 99,[20] and WinGX system, ver. 1.70.01.[21] Selected bond distances and angles for **1** are given in Table S1 in the Supporting Information. The coordinates, anisotropic displacement parameters, and torsion angles for compound **1** are submitted as Supporting Information in CIF format.

Methods of Calculation. We use the Vienna Ab Initio Simulation Package (VASP)[22a,b] implementation of density functional theory (DFT) with PW91 exchange correlation energy of electrons[22c] to describe ionic potential with augmented wave potentials.[22d] The corresponding plane wave expansion of the Kohn−Sham wave function was cut off at 400 eV in calculation. We sampled integration over Brillouin zone with a 2 × 2 × 2 uniform mesh of k-points. We use experimental structural parameters of the dehydrated MOF (Figure 1) as an initial host structure and consider several locations and orientations of H_2 molecule interacting at different sites, such those near K and Ho sites on the pore surface until the structures were relaxed to minimize energy (keeping *a*, *b*, *c* fixed) until Hellmann−Feynman forces are less than 0.02 eV/atom. Cation−oxygen bond lengths in the optimized structure (see the Supporting Information Table S2) are within 2% (typical of DFT calculations) of the experimental values. Thus our pseudopotentials and other calculation parameters should be reasonably reliable.

Results and Discussion

IR Spectroscopy. The IR spectrum of **1** shows bands at 1621 cm^{-1} and 1325 cm^{-1} corresponding to ν_s(COO) and

(18) Sheldrick, G. M. *SHELXL 97, Program for the Solution of Crystal Structure*; University of Göttingen: Göttingen, Germany, 1997.
(19) Sheldrick, G. M. *SHELXS 97, Program for the Solution of Crystal Structure*; University of Göttingen: Göttingen, Germany, 1997.
(20) Spek, A, L. *PLATON, Molecular Geometry Program*; The University of Utrecht: Utrecht, The Netherlands, 1999.
(21) Farrugia, L. J. *J. Appl. Crystallogr.* **1999**, *32*, 837.
(22) (a) Kresse, G.; Hafner, J. *Phys. Rev. B*. **1993**, *47*, 558. (b) Kresse, G.; Furthmuller, J. *Phys. Rev. B* **1996**, *54*, 11169. (c) Perdew, J. P.; Wang, Y. *Phys. Rev. B*. **1992**, *45*, 13244. (d) Bloechl, P. *Phys. Rev. B* **1994**, *50*, 17953.

ν_{as}(COO), respectively of the ox^{2-} ligand coordinated to Ho^{III} and K^{I} atoms.[23] The broadband around 3526 cm^{-1} correspond to the ν(OH) of the water molecules coordinated to K^{I} atom (see Figure S1 in the Supporting Information).

Structural Description of $\{KHo(C_2O_4)_2(H_2O)_4\}_n$ (1). Compound **1** was crystallizes in tetragonal I41/*amd* space group and X-ray structural determination[24] reveals that **1** is a neutral 3D bimetallic coordination architecture of Ho^{III} and K^{I} linked by the oxalate ligand (ox^{2-}), showing the formulation of $\{KHo(C_2O_4)_2(H_2O)_4\}_n$. Each octacoordinated Ho^{III} center chelated to four different ox^{2-} through the oxygen atoms (O1, O2_c; $c = 1/4 + y, 1/4 - x, -1/4 + z$) forming a distorted square-antiprismatic geometry around Ho^{III} center with HoO_8 chromophore (Figure 1a). The resulting $Ho(ox)_4^{5-}$ connected to another four Ho^{III} and eight K^{I} atoms resulting a 3D coordination framework with α-Po type cubic network topology (Figure 1b and Figure S2 in the Supporting Information). Each octacoordinated K^{I} atom ligated to four oxygen atoms (μ_2-O2) from four different ox^{2-} ligands and rest of the coordination is filled by the four water molecules (O3). Therefore, each ox^{2-} functions as a tetradentate μ_4-bridging ligand and connected to two Ho^{III} by chelation and two K^{I} ions through the μ_2-O bridges (Figure 1a). The Ho1−O1 and Ho1−O2 bond distances are 2.339(6) and 2.377(5) Å, respectively, whereas K1−O2 bond distance (2.844(5) Å) is slightly smaller than K1−O3 (2.888(14) Å). In the 3D coordination framework along the crystallographic *c*-axis, octacoordinated K^{I} and Ho^{III} atoms are alternatively positioned through μ_2−O bridges, which are further connected by the ox^{2-} ligands forming square-shaped channels occupied by the four water molecules coordinated to the K^{I} atom (see Figure S2 in the Supporting Information). Removal of the coordinated water molecules from the K^{I} center results in bidirectional channels with the dimensions of 3.6 × 3.6 $Å^2$ along the *c*-axis and 2.0 × 1.2 $Å^2$ along perpendicular to the *a*-axis (b and c in Figure 1 and Figure S3 in the Supporting Information,) and no additional channels were found along *a* and *b*-axis (see Figure S4 in the Supporting Information). The calculation using PLATON suggests that the dehydrated framework contains 30.8% void space to the total crystal volume.[20] The nearest neighbor separations between Ho1−Ho1 through the ox-bridges and Ho1−K1 through the μ_2−O bridges are 6.151 and 4.458 Å, respectively. The compound **1** is one of the very few examples where no additional solvent molecule is attached to the Ho centers to satisfy the high coordination number of the lanthanide ions.

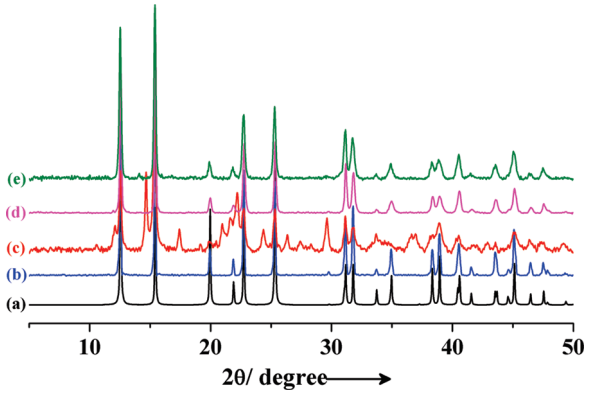

Figure 2. PXRD pattern for $\{KHo(C_2O_4)_2(H_2O)_4\}_n$ (**1**) in different states: (a) simulated from X-ray single crystal data; (b) as-synthesized; (c) at 120 °C under a vacuum; (d) exposed to the H_2O vapor; and (e) CH_3CN vapor.

Framework Stability. To study the framework stability of **1**, we performed TG analysis and powder X-ray diffraction (PXRD) pattern at different temperatures. The TGA study suggests that four K^{I}-bound water molecules are released in the temperature range of 45−120 °C and the dehydrated solid (**1′**) is stable up to 380 °C without further weight loss. The weight loss (obsd 15.01 wt %) is consistent with the four water molecules (calcd 14.16 wt %). The PXRD pattern of **1′** shows sharp lines with shifting of some peak positions, like (101) peak shifted from 2θ = 12.56 to 12.88°, and the appearance of some new peaks in comparison to the as-synthesised framework **1**, suggesting structural transformation after removal of the K-bound water molecules, rather than the collapse of the framework. Indexing of the powder pattern of **1′** by using the TREOR program[25] suggests monoclinic crystal system with a = 14.690(5) Å, b = 11.428(4) Å, c = 7.879(2) Å, β = 91.50(5)°, and V = 1322.39 $Å^3$, which indicates the structural distortion in **1** after removal of the water molecules (see the Supporting Information). When **1′** is exposed to water vapor for three days, the original framework is regenerated as suggested by the PXRD pattern (Figure 2d). Indexing of the powder pattern of the rehydrated solid indicating the tetragonal crystal system with cell parameters $a = b$ = 11.467(7) Å; c = 8.902(5) Å; V = 1170.75 $Å^3$, which is similar to the assynthesized framework **1**.

Adsorption Property. Encouraged by the exceptionally high thermal stability of the dehydrated compound (**1′**), N_2 (77 K) and CO_2 (195 K) adsorption properties were investigated to establish permanent porosity. As shown in Figure 3, the framework exhibits a typical type-II isotherm for N_2 (kinetic diameter 3.6 Å)[26,27] and type-I profile for CO_2 (3.4 Å) adsorption. The surface area calculated from the Langmuir equation is about 69.1 and 324.35 m^2/g for N_2 and CO_2 adsorption profiles,

(23) Nakamoto, K. *Infrared and Raman Spectra of Inorganic and Coordination Compounds*, 5th ed.; John Wiley & Sons: New York; 1997.

(24) Crystal data for $\{KHo(C_2O_4)_2(H_2O)_4\}_n$ (**1**): F_w = $C_4H_8HoKO_{12}$, M_w = 452.07, tetragonal, space group I41/*amd* (No. 141), $a = b$ = 11.4651(3) Å, c = 8.9154(3) Å, V = 1171.92(6) $Å^3$, Z = 4, ρ_{calcd} = 2.517 g cm^{-3}, μ ($Mo_{K\alpha}$) = 7.163 mm^{-1}, F(000) = 824, T = 293 K, λ ($Mo_{K\alpha}$) = 0.71073 Å, θ_{max} = 29.7°, total data = 4285, unique data = 438, R_{int} = 0.089, obsd data [$I > 2\sigma(I)$] = 394, R = 0.0255, R_w = 0.0927, GOF = 1.38.

(25) Werner, P. −E.; Eriksson, L.; Westdahl, M. *J. Appl. Crystallogr.* **1985**, *18*, 367.

(26) Molecular areas are calculated from liquid density, assuming spherical symmetry and a hexagonal close packing. The equation and values are in ref 27.

(27) Webster, C. E.; Drago, R. S.; Zerner, M. C. *J. Am. Chem. Soc.* **1998**, *120*, 5509.

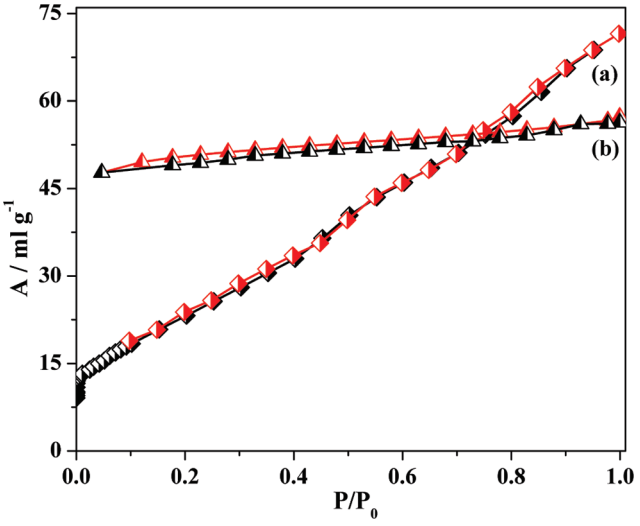

Figure 3. (a) N_2 (at 77 K) and (b) CO_2 (at 195 K) adsorption (black) and desorption (red) isotherms for **1′**. P_o is the saturated vapor pressure of the adsorbates.

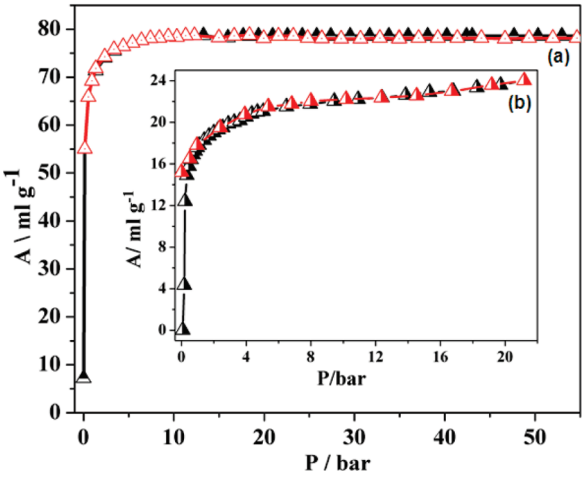

Figure 4. High-pressure H_2 and CO_2 sorption isotherms for **1′**. (a) H_2 at 77 K; (b) CO_2 at 298 K (inset).

respectively. The steep uptake of CO_2 at low-pressure regions suggests strong interaction with the pore surfaces, which is also realized by the high isosteric heat of adsorption (−26.3 kJ/mol) obtained from the Dubinin−Radushkevich (DR) equation.[28] Moderate surface area and highly reactive pore surfaces decorated with unsaturated alkali metal ions (K^I) prompted us to measure H_2 storage capacity of the framework **1′**. High pressure hydrogen sorption at 77 and 195 K were found to be 0.70 and 0.11 wt %, respectively (Figure 4a and Figure S6 in the Supporting Information). Steep uptake of H_2 at low-pressure regions at 77 K is consistent with strong interactions between H_2 molecules and pore surfaces, possibly because of the presence of highly reactive unsaturated K-sites. The framework saturated with respect to H_2 at 16 and 50 bar at 77 and 195 K, respectively (see Figure S6 in the Supporting Information). The heat of hydrogen adsorption was calculated using the Clausius−Clapeyron[13k]

(28) Dubinin, M. M. *Chem. Rev.* **1960**, *60*, 235.

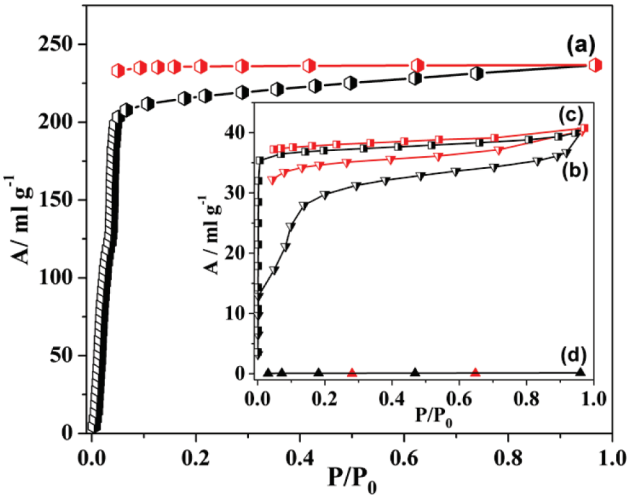

Figure 5. Vapor sorption isotherm for **1′**. (a) H_2O (298 K); (b) MeOH (293 K); (c) CH_3CN (298 K); and (d) EtOH (298 K). P_0 is the saturated vapor pressure of the adsorbates at respective temperature.

Table 1. Calculated Energies and Structural Parameters of Various Configurations of H_2 Molecules Adsorbed in the MOF. Distances are Calculated from the Centre of Mass of H_2 to Metal Sites

structure	ΔH_{ads} (kJ/mol)	H_2−K distance (Å)	H_2−Ho distance (Å)
H_2 in big pore (K is along the H_2 axis)	−7.46	4.72	4.18
H_2 in small pore (K is along the H_2 axis)	+1.23	3.47	4.39
H_2 in big pore (K is on the perpendicular bisector of H_2 axis)	−9.03	3.27	4.68
H_2 in small pore (K is on the perpendicular bisector of H_2 axis)	−10.45	3.07	4.40

equation, suggesting $\Delta H_{ads} = -9.21$ kJ/mol at low coverage regions, which is significantly high among the reported porous metal-organic framework systems.[14c] The density of the adsorbed H_2 was calculated with respect to the total pore volume (0.1042 cm^3/g), giving a value of approximately 0.0672 g/cm^3, which is comparable to liquid hydrogen density (0.0708 g/cm^3), indicating that the H_2 molecules are in compressed state in the channels.[13i] We have also measured H_2 sorption at 77 K up to 1 atm ($P/P_0 \approx 1$), which exhibits a steep uptake at very low pressure regions and ended without saturation (see Figure S7 in the Supporting Information). The sorption is consistent with high-pressure measurement at low-pressure regions. The high-pressure CO_2 adsorption profile shows 4.7 wt % storage capacities at 298 K and 20 bar (Figure 4b), and this value is slightly decreases to 3.47 wt % at low-pressure measurement ($P/P_0 \approx 1$) at 298 K (see Figure S8 in the Supporting Information). Inspired by the square-shaped channel decorated with highly active alkali metal ions, we anticipated that **1′** could selectively adsorb solvent molecules on the basis of size and polarity. H_2O, CH_3CN, and EtOH sorption experiments were carried out at 298 K and MeOH sorption was measured at 293 K (Figure 5). H_2O (kinetic diameter 2.65 Å) and CH_3CN (kinetic diameter 4.0 Å)[26,27] sorption

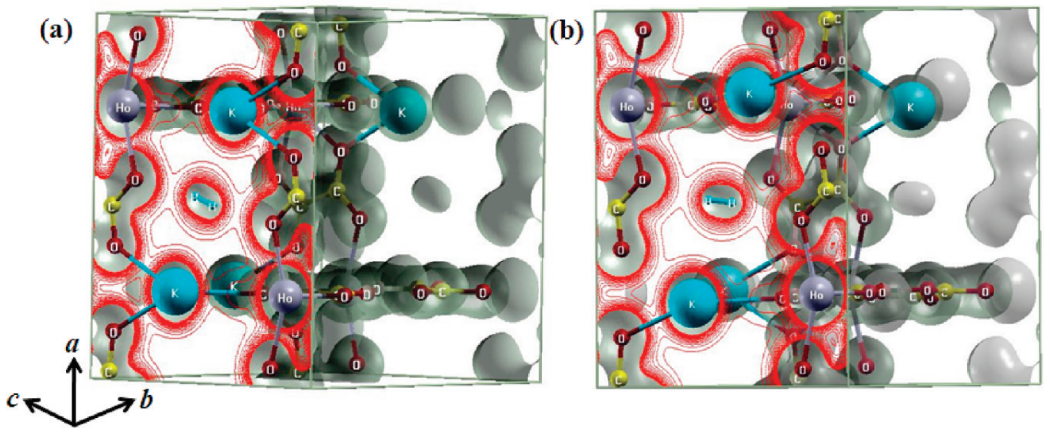

Figure 6. Iso-surfaces of charge density (iso-value = 0.5 a.u.) of the optimized structure of an H_2 molecule adsorbed inside a small pore of the **1′** simulated from first-principles: the molecular axis of H_2 is (a) perpendicular and (b) parallel to the line joining the center of mass of H_2 with K site.

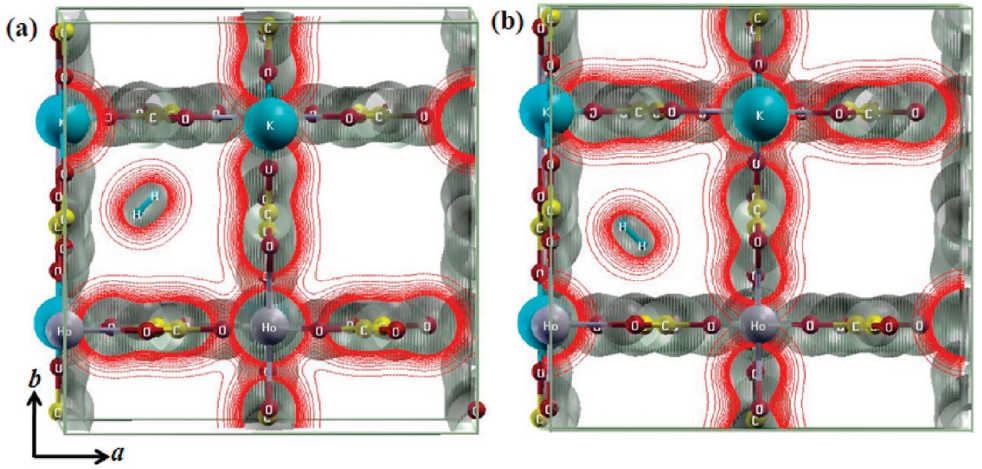

Figure 7. Iso-surfaces of charge density (iso-value = 0.5 a.u.) of the optimized structure of an H_2 molecule adsorbed inside a big square pore of the MOF simulated from first-principles: the molecular axis of H_2 is (a) perpendicular and (b) parallel to the line joining the center of mass of H_2 with K site.

profiles exhibit typical type-I curve (a and c in Figure 5), whereas MeOH (kinetic diameter 3.8 Å) sorption occurs in two-step processes (Figure 5b (inset)). Hysteretic sorption and a rapid rise at the low-pressure region suggest strong interaction with the pore surfaces. The calculations using saturation sorption amount suggest that framework **1′** uptakes 4 molecules of H_2O, 0.4 molecule of MeOH, 0.7 molecule of CH_3CN per formula unit. All the profiles were analyzed by the DR equation and βE_0 values, which reflect the adsorbate−adsorbent affinity, are 5.8, 7.72, and 9.99 kJ/mol for H_2O, CH_3CN, and MeOH, respectively. CH_3CN loaded samples of **1′** reveals similar PXRD pattern as of assynthesized framework, suggesting structural transformation after accommodation of CH_3CN molecules (Figure 2e). IR spectrum of CH_3CN adsorbed sample exhibits additional peaks around 2978 cm^{-1} and 2258 cm^{-1}, corresponding to the ν(C−H) and ν(CN), respectively of CH_3CN molecule (see Figure S9 in the Supporting Information).[23] The higher ν(CN) stretching frequency compare to the free CH_3CN (ν(CN) = 2231 cm^{-1}) suggests that CH_3CN molecules are strongly embedded in the pores decorated with unsaturated K^I sites. Framework **1′** completely excludes EtOH molecules (kinetic diameter 4.3 Å)[27,28] consistent with the smaller pore size in **1′**. The structural reversibility with dehydration and rehydration can be realized by the similar PXRD pattern and the same amount of water adsorption revealed from the sorption profile.

We now use first-principles calculations to understand the ability of the framework to store hydrogen at the different lattice sites through determination of the respective adsorption energies and structures. We used the dehydrated (**1′**) structure of the bimetallic MOF as an initial structure in geometry optimization to obtain the bare MOF structure, and its energy (E(bare MOF)) is used in evaluation of the adsorption energy of hydrogen molecules

$$\Delta H_{ads} = E(\text{MOF with } H_2) - \{E(\text{bare MOF}) + E(H_2)\}$$

Our results for H_2 adsorbed at various sites in the MOF (Table 1) clearly show that the strongest interaction occurs when H_2 is in the small pore and close to K-site (Figure 6a) with an adsorption energy of −10.44 kJ/mol. In this configuration, the K-site lies on the perpendicular bisector of the H_2 bond. In contrast, when the K-site lies along the H_2 molecular axis (Figure 6b), we find the adsorption energy to be positive, showing a strong

dependence of ΔH_{ads} on the orientation of H_2 molecule in the small pore. We have also examined H_2 in large pores and respective adsorption energies and structure (Figure 7). When the K-site lies on the perpendicular bisector of H_2 bond (Figure 7a), the ΔH_{ads} (−9.03 kJ/mol) is lower than that when K-site lies on the H_2 molecular axis (−7.46 kJ/mol) (Figure 7b). When the molecular axis of H_2 in an initial structure is along the line between the center of H_2 and a K-site, the H_2 molecule migrates in relaxation closer to another K-site with its axis perpendicular to the line between its molecular center and the second K site (Figure 7b). This is consistent with lower energies associated with geometry with perpendicular axis of H_2 and stronger adsorption energies of these two configurations. It is worth mentioning that our theoretically observed ΔH_{ads} values agree well with the experimental finding. Analyses of different inter atomic distances (Table 1) in all the configurations shows that H_2 molecule is always closer to K^I-site than Ho^{III} site. Interestingly, even with the initial configuration of H_2 adsorbed near the Ho-site relaxes to a lower-energy configuration where H_2 migrates to K-site. This shows that in **1′** K^I is the preferential site of adsorption, and there is no energy barrier for migration of H_2 from Ho^{III} center to K^I-site.

In the optimized structures of H_2 adsorbed in the MOF, our estimate of the H_2 molecular bond length varies from 0.751 to 0.757 Å. With our theoretical estimate of the bond length of isolated H_2 molecule of 0.75 Å, it is quite clear that the interaction of H_2 with MOF is not chemisorptive. The interaction between H_2 molecule and the MOF lattice with unsaturated metal (K^I) site is largely electrostatic in nature.[14j] The van der Waals interaction is not captured in our theoretical description of the H_2−MOF interaction based on DFT-PW91 approximation, which is expected to be weakly negative at a distance of about 3.8 Å between H_2 molecule and the MOF lattice. However, DFT calculations are known to overestimate the binding energies, and hence our estimates of binding energies are close the experimental estimates. We note that our theoretical analysis also ignores thermal contributions to the free energy of binding or its pressure dependence, which could also partly compensate the errors in our estimates of adsorption energies.

Conclusion

In conclusion, we have successfully synthesized a new bimetallic (Ho^{III}−K^I) 3D α-Po type framework with bidirectional channels by making use of oxalate as an organic linker. The dehydrated framework (**1′**) shows permanent porosity and good H_2 and CO_2 storage capacity at high pressure and low temperature. The framework **1′** shows high heat of H_2 sorption (approximately −10 kJ/mol), realized by the interactions with unsaturated K-sites, which is confirmed quantitatively using first-principles calculations. Through first-principles DFT simulations, we show that a hydrogen molecule preferentially adsorbs (a) near a K-site than a Ho-site, and (b) with its axis perpendicular to the line joining K-site and its center. We suggest a recipe to develop better hydrogen storage materials through incorporation of unsaturated and reactive alkali metal ion in the pore surfaces of metal organic frameworks. The vapor sorption studies reveal easy uptake of H_2O, MeOH, and CH_3CN molecules, but completely excludes EtOH molecules, may find industrial application in discriminating the MeOH molelcule from a mixture of MeOH and its higher homologues.

Acknowledgment. T.K.M. acknowledges the financial support from DST (fast-track proposal) and K.P.S.S.H. acknowledges support from a DRDO grant. S.M. is thankful to CSIR for financial support.

Supporting Information Available: IR, different crystallographic figures, TGA, and adsorption figures (Figure S1−S9, PDF); crystallographic information files (CIF). This material is available free of charge via Internet at http://pubs.acs.org